Volume 27
Number 13
7 April 2025
Pages 1853–2034

CrystEngComm

rsc.li/crystengcomm

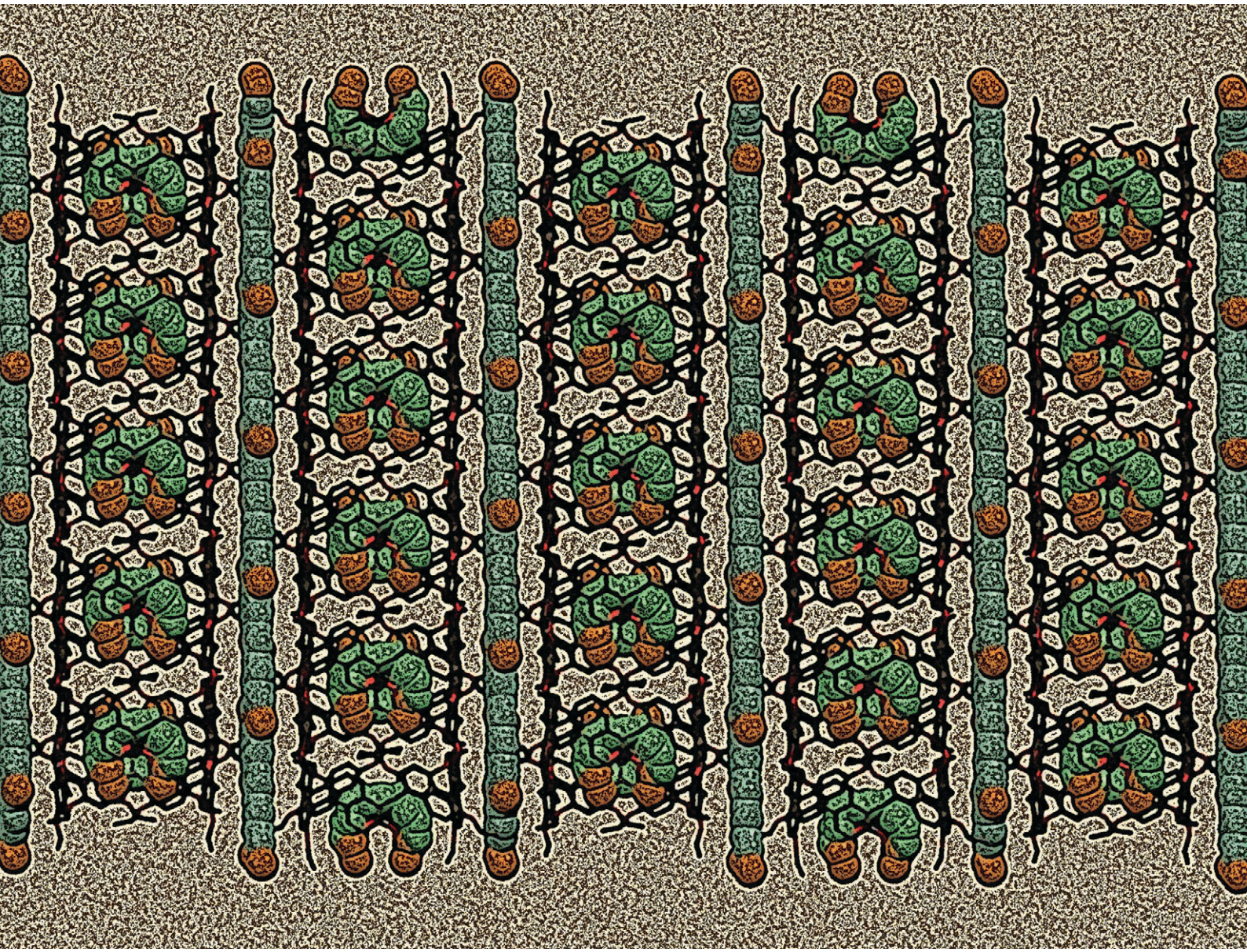

ISSN 1466-8033

ROYAL SOCIETY OF CHEMISTRY

PAPER

Talal F. Al-Azemi *et al.*

Prism[*n*]arene-alkyl dibromide (*n* = 5, 6) synergy: molecular affinity in the solid state

CrystEngComm

ROYAL SOCIETY OF CHEMISTRY

PAPER

View Article Online
View Journal | View Issue

Cite this: *CrystEngComm*, 2025, **27**, 1873

Prism[*n*]arene-alkyl dibromide (*n* = 5, 6) synergy: molecular affinity in the solid state†

Mickey Vinodh, Nour O. Abdeljaber, Fatemeh H. Alipour and Talal F. Al-Azemi *

Received 28th December 2024,
Accepted 25th February 2025

DOI: 10.1039/d4ce01320d

rsc.li/crystengcomm

Single crystals of prism[5]arene and prism[6]arene were grown from solutions containing either 1,6-dibromohexane or 1,8-dibromooctane. The deeper cavity of the prism[5]arene macrocycle efficiently encapsulated longer alkyl dibromide guests compared to pillar[5]arene, forming 1 : 1 inclusion complexes stabilized by multiple C–H···π and C–H···O interactions. Both inclusion complexes self-assembled into linear supramolecular polymers within the crystal network, facilitated by guest halogen interactions (C–H···Br and Br···Br interactions). Prism[6]arene co-crystals grown from 1,6-dibromohexane and 1,6-dibromooctane formed a unique 1 : 1 inclusion complex, where the guest adopted an orthogonal orientation within the host cavity. The resulting supramolecular assemblies were fully characterized using single-crystal X-ray diffraction and Hirshfeld surface analysis.

Introduction

Phenol-based macrocyclic arenes, such as calix[*n*]arenes, have long been recognized as efficient macrocyclic hosts in molecular recognition and supramolecular chemistry.[1,2] In contrast, naphthol-based macrocyclic arenes remain underexplored. There are a few relevant literature works related to calix[*n*]naphthalenes, which are a class of naphthol-based macrocycles with 1,6-dimethoxynaphthalene units linked by methylene bridges at their *meta* positions.[3–6] Another hybrid class, calix[2]naphtha[2]arene, combines the conformational and recognition properties of calixarene and naphthalene macrocycles.[7] Macrocycles based on naphthol units offer advantages over conventional calix[*n*]arenes, including deeper and more electron-rich cavities and inherent chirality.[6]

Pillar[*n*]arenes, in contrast, demonstrate a rigid architecture and exceptional host–guest properties. Moreover, they offer various cavity sizes (*n* = 5, 6, 7 and 10) and are relatively straightforward to modify and functionalize, making them highly versatile materials suitable for a broad spectrum of applications.[8–11] Similar to pillar[*n*]arenes, the recently reported prism[*n*]arenes differ by having dimethoxybenzene units replaced with dimethoxynaphthalene units.[12,13] The family of prism[*n*]arenes is a small family, having two members which are prism[5]arene and prism[6]arene, analogues to their pillar[5]arene and pillar[6]arene counterparts. Another class of macrocyclic arenes, called pagoda[*n*]arenes, has been reported in 2020. These macrocycles have fluorescence properties in addition to deep electron rich cavities resulting from the replacement of the dimethoxybenzene units, found in pillar[*n*]arenes, with dimethoxyanthracene ones. This was done in the aim of utilizing the interesting features of incorporating anthracene into the macrocyclic scaffold. Similarly, the newly discovered family consists of two members: pagoda[4]arene and pagoda[5]arene.[14,15]

The inherited fluorescence properties of naphthalene or anthracene units in the macrocyclic backbone enable their utility in detection and sensing applications. In addition, their large π system provides a deeper and electron rich cavity, enhancing its host–guest properties. Another effect will be increasing the structural complexity, which may result from the low symmetry of naphthalene.[16] Reports indicate that the permethylated prism[5]arene exhibits a prism shape with a bulky ammonium guest, while the ethyl-prism[6]arene adopts a folded cuboid shape when its induced by a suitable guest.[12,13] However, detailed structural investigation of these prism[*n*]arene systems, particularly during host–guest interactions and their supramolecular characteristics, is still underdeveloped.[17–19] Following our continuous efforts in studying macrocyclic arenes with different cavity shapes and sizes, we have recently reported the host–guest properties of pillar[5]arene and pagoda[4]arene with α,ω-dibromoalkanes and their linear supramolecular polymer assembled *via* halogen–halogen interactions both in solution and in the solid state.[20,21] Moreover, the effect of the crystallization solvent on the supramolecular self-assemblies of pillar[5]arene has been studied, along with a comparison to their behavior in solution.[22]

Chemistry Department, Kuwait University, P.O. Box 5969, Safat 13060, Kuwait. E-mail: t.alazemi@ku.edu.kw

† Electronic supplementary information (ESI) available. CCDC 2405326–2405329. For ESI and crystallographic data in CIF or other electronic format see DOI: https://doi.org/10.1039/d4ce01320d

In this present work, we report the crystal structures of host–guest inclusion complexes and their corresponding supramolecular self-assemblies based on permethylated-prism[5]arene (**PS-5**) and perethylated-prism[6]arene (**PS-6**), co-crystallized with 1,6-dibromohexane (**DBH**) and 1,8-dibromooctane (**DBO**). The influence of the guest molecules and the host cavity on the supramolecular self-assemblies in the solid state is investigated. For the prism[5]arene host, the supramolecular polymer assembly, driven by guest halogen-bond interactions, is influenced by the alkyl bromide guest length. In contrast, the cavity of prism[6]arene exhibits distinct behavior toward the linear guests. A detailed characterization of the supramolecular interactions within the crystal network is provided.

Experimental

Prism[5]arene (**PS-5**) and prism[6]arene (**PS-6**) were synthesized according to previously reported procedures.[12,13] Single-crystal data collection was performed on a Bruker X8 Prospector diffractometer (Germany) using Cu-Kα radiation at room temperature. The reflection frames were integrated using the Bruker SAINT software package with a narrow-frame algorithm. The structure was subsequently solved using the Bruker SHELXTL software package and refined with SHELXL-2019/3.[23] All non-hydrogen atoms were refined anisotropically, while hydrogen atoms were placed at calculated positions and refined using the riding model. The hydrogen atom which is involved in the Br···H interaction in [**PS-5** ⊃ **DBH**] has been assigned directly from the electron density map. The disordered alkyl dibromide molecules in [**PS-5** ⊃ **DBH**] and [**PS-6** ⊃ **DBO**], which occupy special positions, were refined using the PART-1 instruction with 50% occupancy for two positions of the guest molecules. Molecular graphics and the calculation of intermolecular interactions were conducted using Mercury (ver. 2024.3.0), while Hirshfeld surface analysis was performed using CrystalExplorer 21.5.[24]

Preparation of single crystals for X-ray diffraction

Single crystals of the **PS-5**/1,6-dibromohexane inclusion complex were grown by dissolving **PS-5** (10 mg) in a solution of dichloromethane and 1,6-dibromohexane (1 mL, 90 : 10; v/v), followed by slow solvent evaporation under controlled conditions. Single crystals suitable for X-ray diffraction analysis were obtained within 5 days. Similarly, single crystals of the **PS-5**/1,8-dibromooctane inclusion complex were grown by dissolving **PS-5** (10 mg) in a solvent system of dichloromethane and 1,8-dibromooctane (1 mL, 90 : 10; v/v) under similar conditions. For the **PS-6**/1,6-dibromohexane and **PS-6**/1,8-dibromooctane inclusion complexes, crystals were grown by dissolving **PS-6** (10 mg) in a solvent system of dichloromethane and 1,6-dibromohexane or 1,8-dibromooctane (0.5 mL, 90 : 10; v/v), followed by slow solvent evaporation under controlled conditions. The crystallographic data for the structures reported in this paper have been deposited at the Cambridge Crystallographic Data Centre (CCDC 2405326–2405329).

Results and discussion

The depth of a macrocyclic arene plays a crucial role in its ability to encapsulate long-chain alkyl bromides. A deeper cavity in the macrocycle enhances the accommodation of longer alkyl chains, allowing for more effective host–guest interactions. This structural feature provides increased spatial confinement, which promotes stronger van der Waals interactions and better stabilization of the encapsulated molecule in the electron-rich environment of the arene cavity, enhancing the encapsulation efficiency. The depth and shape of the macrocycle can therefore influence selectivity and binding strength, making it a key factor in designing macrocyclic hosts for long-chain alkyl bromides. Another key factor influencing the encapsulation properties of arene macrocycles toward long-chain alkyl bromides is the size and the shape of their cavity, which directly impacts the strength of van der Waals interactions within the cavity. The chemical structure representations of the inclusion complexes based on prism[5]arene and prism[6]arene with alkyl dibromide guests are illustrated in Fig. 1.

To explore the host–guest properties, suitable single crystals for X-ray diffraction analysis were grown by the co-crystallization of prism[*n*]arene macrocycles (*n* = 5 or 6) with 1,6-dibromohexane (DBH) or 1,8-dibromooctane (**DBO**). The crystal structures of the inclusion complexes [**PS-5** ⊃ **DBH**] and [**PS-5** ⊃ **DBO**], obtained from solutions containing dichloromethane/DBH or DBO, are illustrated in Fig. 2. Detailed crystallographic features are provided in Table S1 of the ESI.† The crystal structures reveal prism[5]arene macrocycles encapsulating either **DBH** or **DBO** within their cavities, forming a 1 : 1 inclusion complex stabilized by C–H···π and C–H···O interactions. The threading of the dibromoalkane guest molecules inside the prism[5]arene cavity closely resembles the encapsulation behavior observed in structurally similar pillararene inclusion complexes.[17] However, the **DBH** molecule encapsulated within the cavity of [**PS-5** ⊃ **DBH**] lies on a two-fold rotation axis and exhibits positional disorder. The refinement of this disorder, which involves a special position, was performed using the PART-1 instruction, assigning 50% occupancies to two positions of the **DBH** guest molecule (Fig. 3a). The positional disorder exhibited by the **DBH** guest molecules suggests their inherent flexibility, allowing them to occupy multiple sites within the prism[5]arene cavity. This behavior can be attributed to the larger cavity opening size of

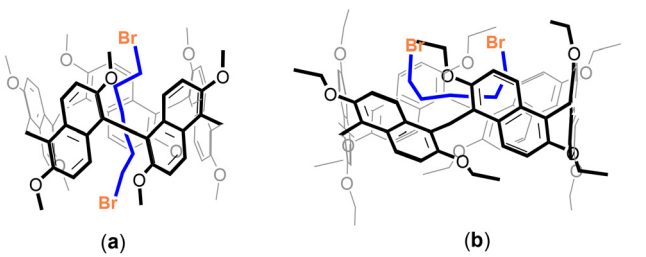

Fig. 1 Chemical structure representations of the inclusion complexes based on prism[5]arene (a) and prism[6]arene (b), with 1,6-dibromohexane (**DBH**) guest.

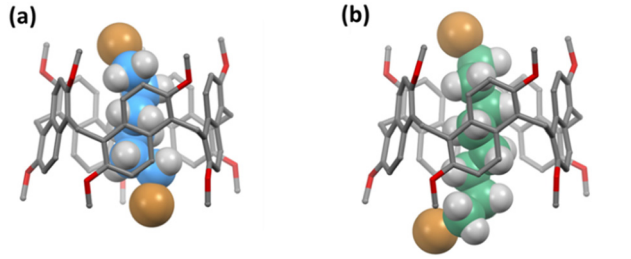

Fig. 2 Crystal structures of the inclusion complexes based on prism[5]arene with 1,6-dibromohexane (**DBH**) (a), and 1,8-dibromoctane (**DBO**) (b), showing higher occupancy guest conformations.

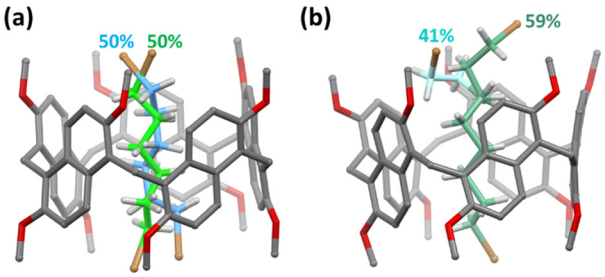

Fig. 3 Crystal structures of the inclusion complexes based on prism[5]arene with 1,6-dibromohexane (**DBH**) (a), and 1,8-dibromooctane (**DBO**) (b), showing percent occupancy guest conformations.

prism[5]arenes (71.4 Å^2) compared to their structurally analogous pillar[5]arenes (58.6 Å^2).[18] For the longer guest molecule in the inclusion complex, [**PS-5** ⊃ **DBO**] exhibits positional disorder only in the extended end-chain outside the cavity, with occupancy ratios of 59% and 41% (Fig. 3b). Quantitative details of the non-bonding interactions experienced by the encapsulated guests are summarized in Tables S2 and S3.†

Self-assembled supramolecular polymer

Among the non-bonding interactions C–H···π, C–H···O, C–H···Br, and Br···Br in the inclusion complex crystals, the C–H···Br and Br···Br interactions are particularly significant. These interactions align along a linear chain within the crystal lattice, promoting the formation of a linear supramolecular prism[*n*]arene polymer within the crystal network. However, due to positional disorder experienced by guest molecules in the inclusion crystals, accurate quantification of the Br···Br and Br···H interactions is not feasible. When considering only one of the disordered **DBH** fragment of the disordered structure, the supramolecular polymer based on [**PS-5** ⊃ **DBH**] assembled in the solid state by intermolecular Br···H interactions between the encapsulated guest and aromatic hydrogen of the adjacent prism[5]arene at one end and by intermolecular Br···Br interactions between the encapsulated guests at the other end as shown in Fig. 4a. The intermolecular Br···H anchor interactions have separations of 3.05 Å, which corresponds to the sum of their respective atomic van der Waals radii (3.05 Å). The Br···Br with a measured separation distance of 2.90 Å is

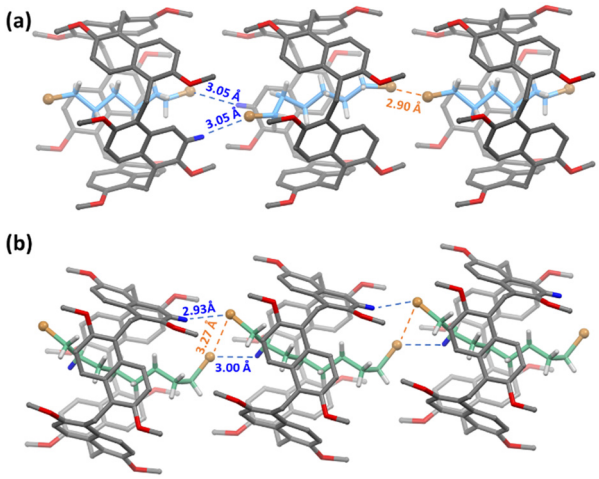

Fig. 4 Crystal structures of the linear supramolecular polymer backbone driven by the guest in the inclusion complexes of [**PS-5** ⊃ **DBH**] (a) and the higher occupancy guest conformation in [**PS-5** ⊃ **DBO**] (b).

unusually short, approximately 21.6% less than the expected van der Waals distance of 3.7 Å, suggesting the presence of a halogen bond with strong partial covalent character. The bond length contraction in halogen–halogen interactions, particularly for Br···Br, I···I, and Cl···Cl bonds is often observed in XRD studies to be shorter than the sum of van der Waals radii. Large bond length contraction (≈25%) were reported for I···I interactions in polyiodides (I_3^-, I_5^-) with bond length contraction between 2.92–3.00 Å of the van der Waals distance (3.96 Å).[25]

In the inclusion complex [**PS-5** ⊃ **DBO**], the major occupancy fragment (59%) of the disordered structure reveals a self-assembled supramolecular polymer within the crystal network, driven by Br···Br and C–H···Br non-covalent interactions. The intermolecular Br···Br distance is calculated to be 3.27(1) Å, which is approximately 11.6% shorter than the sum of the van der Waals radii of bromine atoms (3.7 Å). This indicates strong halogen–halogen interactions with a type II halogen–halogen interaction, based on the geometrical C–X···X–C angles (θ_1 and θ_2). The self-assembled supramolecular polymer was further consolidated by C–H···Br interactions between the guest–guest and the guest–host hydrogens with measured distances of 2.93 Å and 3.00 Å respectively (Fig. 4b).

The self-assembled supramolecular polymer based on [**PS-5** ⊃ **DBO**], containing a guest fragment with 41% occupancy disorder, exhibits head-to-head Br···H interactions between adjacent inclusion complexes, with a measured separation distance of 2.82 Å (Fig. S9†).

Prism[6]arene on the other hand, exhibits a cuboid shape, with the longer sides comprising two naphthalene units each (12.17 Å) and the shorter sides consisting of a single naphthalene unit (6.45 Å). This unique structural arrangement plays a key role in determining its encapsulation properties. The crystal structures of prism[6]arene, obtained from solutions containing 1,6-dibromohexane and 1,8-dibromooctane, reveal

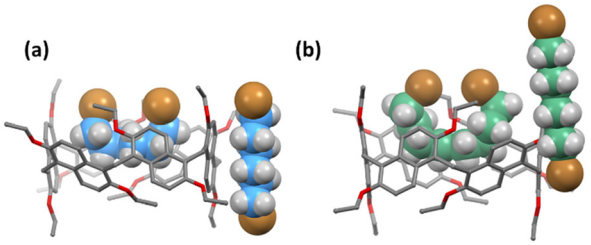

Fig. 5 Crystal structures of the inclusion complexes based on prism[6]arene with 1,6-dibromohexane (**DBH**) (a), and 1,8-dibromohexane (**DBO**) (b), showing major occupancy guest conformations.

that the shape of the cavity plays a crucial role in determining its encapsulation characteristic relative to the length of the alkyl dibromide. Similar to its prism[5]arene analogue, prism[6]arene crystallizes from the 1,6-dibromohexane solution by encapsulating the dibromohexane molecule within its cavity, forming a 1 : 1 inclusion complex. The apt alkyl chain length in guest **DBH** is oriented horizontally along the longer axis of the cavity, while the bromine atoms are positioned perpendicular to the opening of the macrocyclic cavity. This arrangement facilitates multiple non-bonding interactions, including C–H···π, C–H···O, and C–H···Br interactions (Fig. 5a). This orthogonal orientation configuration differs from the threaded encapsulation typically observed in pillar[5]arene,[17] pagoda[4]arene,[18] and prism[5]arene.[12] The crystal obtained from the 1,8-dibromooctane solution exhibits similar incorporation behavior of the guest 1,8-dibromooctane inside the prism[6]arene cavity, adapting an orthogonal orientation (Fig. 5b). The **DBO** guest resides on a two-fold rotation axis and exhibits positional disorder. Similar to the [**PS-5** ⊃ **DBH**] complex, the refinement of this disorder involving special position which was carried out using the PART-1 instruction with 50% occupancies for two positions of the **DBO** guest molecule. The longer alkyl chain of the guest molecule in [**PS-6** ⊃ **DBO**] is more constrained within the macrocycle cavity, with the CH_2–Br ends of the DBO guest oriented perpendicularly. This curvature of the guest molecule led to intermolecular Br···H–C interactions (2.82 Å) with an adjacent prism[6]arene inclusion complex in the crystal network (Fig. S10†). Multiple attempts to crystallize prism[6]arene from a solution containing 1,4-dibromobutane were unsuccessful, likely due to the poor stability of the prism[6]arene–1,4-dibromobutane system. This observation suggests that prism[6]arene exhibits a high level of specificity for guest molecules in the formation of host–guest systems. Notably, in both crystal structures obtained from 1,6-dibromohexane and 1,8-dibromooctane, a corresponding alkyl dibromide molecule co-crystallizes within the void space of the lattice, serving as a space-filling solvent for each prism[6]arene unit (Fig. 5).

Hirshfeld surface analysis

Hirshfeld surface analysis is a powerful method for examining intermolecular interactions experienced by atoms within crystal structures. This analysis features two key components: (1) the 3D d_{norm} surface, which enables visualization and analysis of intermolecular interactions within the crystal, and (2) 2D fingerprint plots, which provide quantitative information on nature and proportion of various intermolecular interactions. On the 3D d_{norm} surface of a crystal, red regions indicate intermolecular contacts shorter than the sum of the corresponding van der Waals radii, white regions denote contacts close to van der Waals distances, and blue regions correspond to contacts longer than the sum of the van der Waals radii. For the [**PS-5** ⊃ **DBH**] and [**PS-5** ⊃ **DBO**] crystals, positional disorder required structural remodeling to generate accurate Hirshfeld surfaces. This was achieved by selecting only the disordered components with the highest occupancy in the [**PS-5** ⊃ **DBO**] complex and the disordered guest in the [**PS-5** ⊃ **DBH**] complex that exhibits C–H···Br interactions. This approach ensures a more accurate representation of intermolecular interactions in the Hirshfeld surface analysis.

The Hirshfeld surface (HS) of [**PS-5** ⊃ **DBH**] shows an intense red spot observed at the opening of one end of the cavity, which corresponds to an unusual bond contraction associated with Br···Br interactions between adjacent **DBH** guest molecules (Fig. 6a). The relatively weak Br···H interactions at the other side of the cavity is evidenced by the white spots on the 3D d_{norm} surface, which is consistent with the larger separation distances observed. For [**PS-5** ⊃ **DBH**], the Hirshfeld surface (HS) region corresponding to the macrocyclic cavity predominantly appears white, indicating the presence of only moderate non-bonding interactions within the cavity. In contrast, the intense red spots observed inside the cavity of [**PS-5** ⊃ **DBO**] suggest a strong fit of the guest molecule within the cavity (Fig. S11†).

The 2D fingerprint plots reveal that the primary intermolecular interactions in the [**PS-5** ⊃ **DBH**] crystals are H···H (57.5%), C···H (18.5%), O···H (9.1%), Br···H (9.8%) and Br···Br (1.8%). In the crystal structure, the major intermolecular interactions, as depicted by the 2D fingerprint plots, are H···H (60.0%), C···H (18.8%), O···H (9.4%), and Br···H (8.6%). The Hirshfeld surface (HS) of [**PS-5** ⊃ **DBO**] exhibits prominent red spots at the center of the prism[5]arene cavity opening, indicating dominant Br···Br and Br···H interactions in the crystal (Fig. 6b). The 2D fingerprint plots reveal that the primary intermolecular interactions in the [**PS-5** ⊃ **DBO**] crystals are H···H (61.1%), C···H (18.1%), O···H

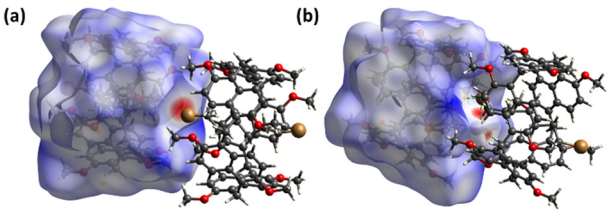

Fig. 6 Hirshfeld surfaces (mapped with d_{norm}) demonstrating the interaction modes of [**PS-5** ⊃ **DBH**] (a) and [**PS-5** ⊃ **DBO**] (b). The red spots at the center of the cavity opening indicate strong Br···Br and Br···H interactions.

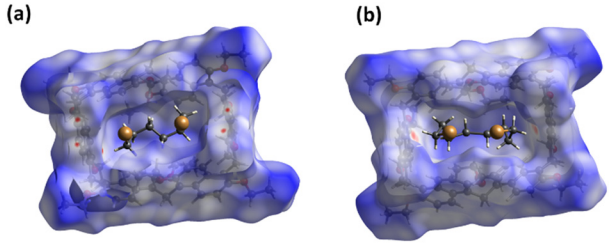

Fig. 7 Hirshfeld surfaces (mapped with d_{norm}) illustrating the interaction modes presented from the top view of [**PS-6** ⊃ **DBH**] (a) and of [**PS-6** ⊃ **DBO**] (b).

(9.1%), and Br···H (7.6%). Notably, Br···Br interactions contribute 0.8% to the total intermolecular interactions. While this percentage is relatively small, it remains significant given that only two bromine atoms are present in the asymmetric unit of the crystal. The Hirshfeld surface analysis confirms the significance of Br···Br and Br···H bonding in the self-assembly of both co-crystal networks.

On the other hand, the cuboid-shaped cavity of **PS-6** effectively encloses the **DBH** and **DBO** guests, with strong C–H···π interactions observed along the narrower sides of the cavity with both end methylene hydrogens. This interaction is evidenced by the presence of intense red spots on the 3D Hirshfeld surface, as depicted in Fig. 7. Moderate interactions along the longer sides of the cavity are depicted on the Hirshfeld surface (HS) as white spots, corresponding to O···H and C–H···π bonds, as well as Br···H interactions with the ethyl substituents on the rim of the cavity. These interactions collectively contribute to a tighter fit of the guest molecule within the cavity.

Conclusions

In summary, we presented four crystal structures based on prism[5]arene and prism[6]arene, incorporating either 1,6-dibromohexane or 1,8-dibromooctane within their crystal networks. The crystal structures were fully characterized *via* X-ray diffraction analysis, revealing that the supramolecular assembly of these structures is influenced by the size and shape of the macrocyclic cavity and the structure of the guest molecules, which play a critical role in the crystal network formation. Prism[5]arene formed a 1 : 1 inclusion complex with both 1,6-dibromohexane and 1,8-dibromooctane. Both alkyl dibromide guests in the prism[5]arene inclusion complexes exhibited positional disorder due to the larger cavity opening of prism[5]arene compared to pillar[5]arene and pagoda[4]arene. The C–H···Br and Br···Br interactions have been found to be particularly important in the formation of self-assembled linear supramolecular polymer in the crystal network. In contrast, prism[6]arene formed a 1 : 1 inclusion complexes with both 1,6-dibromohexane, and 1,8-dibromooctane. The encapsulated alkyl dibromide guests within the cavity of prism[6]arene adopts an orthogonal orientation relative to the macrocyclic cavity, a distinctive feature rarely observed in host–guest systems. The intermolecular interactions within the crystal network were further analyzed using Hirshfeld surface analysis, providing a comprehensive assessment of the nature and extent of interactions experienced by the constituent atoms within the crystal lattice. Ongoing studies in our laboratories aim to explore supramolecular self-assemblies with a broader range of macrocyclic arenes and guest compounds.

Data availability

The data supporting this article have been included as part of the ESI,† and crystallographic data for the four crystals have been deposited at the CCDC under 2405326–2405329 and can be obtained from **https://www.ccdc.cam.ac.uk/**.

Conflicts of interest

There are no conflicts to declare.

Acknowledgements

The support received from the Kuwait University, made available through research grant no. SC 05/23, and the facilities at the RSPU (grant no. GS01/01, GS01/03, and GS03/08) are gratefully acknowledged.

References

1 R. Cacciapaglia, L. Mandolini and R. Salvio, Supramolecular Catalysis by Calixarenes, in *Comprehensive Supramolecular Chemistry II*, ed. J. Atwood, Elsevier, Oxford, 2017, vol. 1, pp. 459–478.
2 E. S. Español and M. M. Villamil, *Biomolecules*, 2019, **9**, 90, DOI: **10.3390/biom9030090**.
3 L.-P. Yang, W.-E. Liu and W. Jiang, *Tetrahedron Lett.*, 2016, **57**, 3978–3985.
4 Y.-F. Wang, H. Yao, L.-P. Yang, M. Quan and W. Jiang, *Angew. Chem., Int. Ed.*, 2022, **61**, e202211853, DOI: **10.1002/anie.202211853**.
5 Y.-F. Ye, H.-Y. Zhang, F. Li, W.-W. Yang, B.-P. Luo and Y.-B. Wang, *J. Org. Chem.*, 2022, **87**, 12132–12147.
6 T. Boinski, A. Cieszkowski, B. Rosa, B. Leśniewska and A. Szumna, *New J. Chem.*, 2016, **40**, 8892–8896.
7 R. D. Regno, P. D. Sala, A. Spinella, C. Talotta, D. Iannone, S. Geremia, N. Hickey, P. Neri and C. Gaeta, *Org. Lett.*, 2020, **22**, 6166–6170.
8 T. Ogoshi, S. Kanai, S. Fujinami, T. A. Yamagishi and Y. Nakamoto, *J. Am. Chem. Soc.*, 2008, **130**, 5022–5023.
9 C. Han, F. Ma, Z. Zhang, B. Xia, Y. Yu and F. Huang, *Org. Lett.*, 2010, **12**, 4360–4363.
10 Z. Li, J. Yang, J. He, Z. Abliz and F. Huang, *Org. Lett.*, 2014, **16**, 2065–2069.
11 T. Ogoshi, K. Masaki, R. Shiga, K. Kitajima and T.-A. Yamagishi, *Org. Lett.*, 2011, **13**, 1264–1266.
12 P. D. Sala, R. D. Regno, L. D. Marino, C. Calabrese, C. Palo, C. Talotta, S. Geremia, N. Hickey, A. Capobianco, P. Neri and C. Gaeta, *Chem. Sci.*, 2021, **12**, 9952–9961.

13 P. D. Sala, R. D. Regno, C. Talotta, A. Capobianco, N. Hickey, S. Geremia, M. D. Rosa, A. Spinella, A. Soriente, P. Neri and C. Gaeta, *J. Am. Chem. Soc.*, 2020, **142**, 1752–1756.
14 X.-N. Han, Y. Han and C.-F. Chen, *J. Am. Chem. Soc.*, 2020, **142**, 8262–8269.
15 X.-N. Han, Q.-S. Zong, Y. Han and C.-F. Chen, *CCS Chem.*, 2021, **3**, 738–750.
16 H. Yao and W. Jiang, Naphthol-Based Macrocycles, *Handbook of Macrocyclic Supramolecular Assembly*, 2019, pp. 1–21.
17 G. Zhang, Z. Li, Z. Pan, D. Zhao and C. Han, *New J. Chem.*, 2023, **47**, 18910–18913.
18 R. D. Regno, P. D. Sala, N. Hickey, S. Geremia, C. Talotta, P. Neri and C. Gaeta, *Eur. J. Org. Chem.*, 2023, **26**, e202300608.
19 R. D. Regno, P. D. Sala, N. Hickey, S. Geremia, C. Talotta, P. Neri and C. Gaeta, *Org. Chem. Front.*, 2024, **11**, 2710–2719.
20 T. F. Al-Azemi and M. Vinodh, *Polym. Chem.*, 2020, **11**, 3305–3312.
21 N. O. Abdeljaber, M. Vinodh and T. F. Al-Azemi, *Tetrahedron*, 2023, **132**, 133240, DOI: **10.1016/j.tet.2022.133240**.
22 M. Vinodh and T. F. Al-Azemi, *CrystEngComm*, 2024, **26**, 5138–5143.
23 G. M. Sheldrick, *Acta Crystallogr., Sect. C: Struct. Chem.*, 2015, **71**, 3–8.
24 M. J. Turner, J. J. McKinnon, S. K. Wolff, D. J. Grimwood, P. R. Spackman, D. Jayatilaka and M. A. Spackman. *CrystalExplorer 21.5*, University of Western Australia, 2021, **https://hirshfeldsurface.ne**.
25 P. H. Svensson and L. Kloo, *Chem. Rev.*, 2003, **103**, 1649–2079.